Supplementary Figures

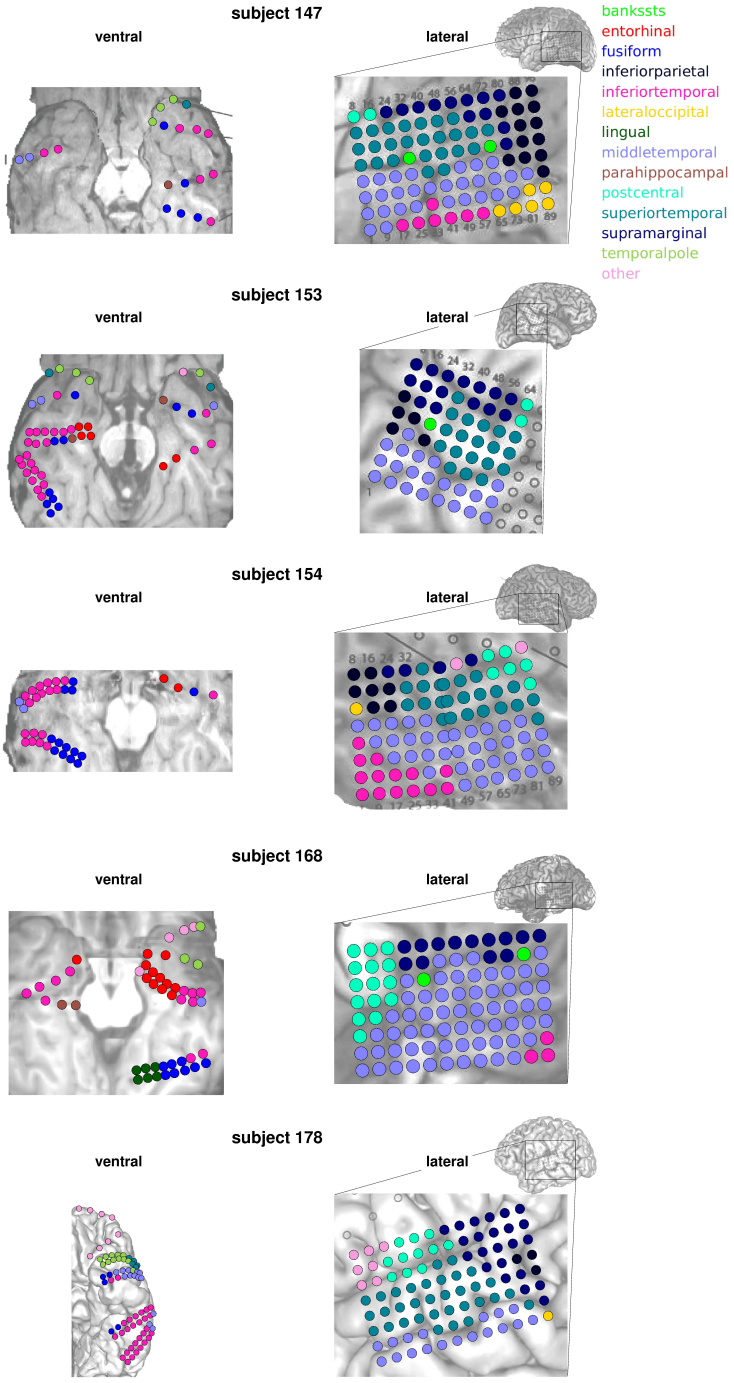

Figure S1: Electrode location for each subject. For each subject, electrodes are color-coded according to their location as returned by an automatic parcellation performed with Freesurfer using the "Desikan-Killiany-Tourville" (DKT) brain atlas, which has been subsequently inspected visually for correspondence with known anatomical landmarks. The label "other" comprises regions that were rarely recorded and did not include discriminant electrodes: these were lateral orbitofrontal cortex, pars orbitalis, precentral cortex, rostral middle frontal cortex, white matter. Subject 168 presented an abnormal anatomy in the lateral temporal lobe. Hence, accurate assessment of the boundary between middle-temporal and superior-temporal cortex was not possible, and the four anterior ventral electrodes labeled as "other" could not be accurately localized.

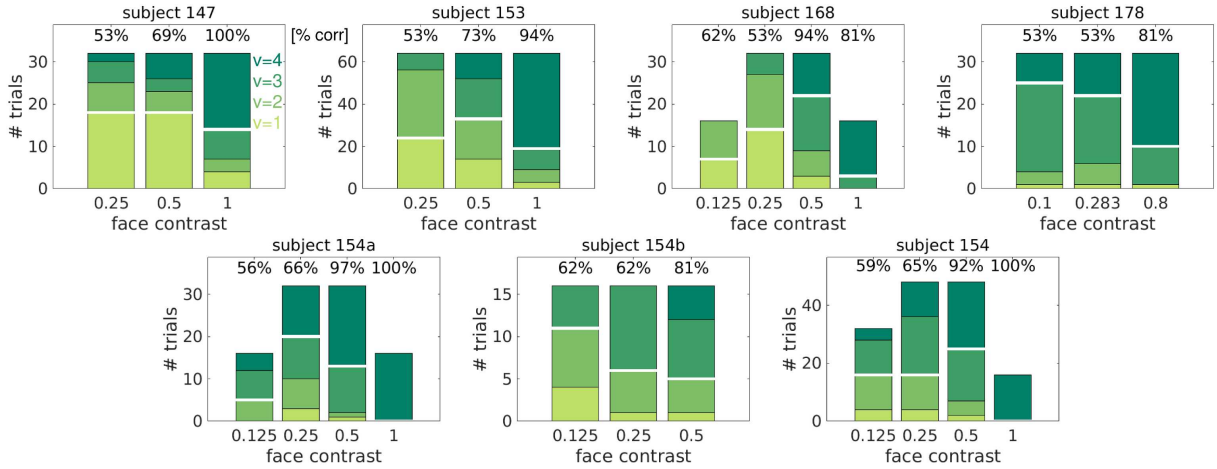

Figure S2: CFS behavioral results for each subject. The stacked bar plots show, for each contrast value, the number of trials that have been assigned to each visibility rating. Color code as in Fig. 2E,F. Numbers on top of each bar show the objective performance (percentage of correct trials over all trials) for each contrast value. In the case of subject 154, the set of recorded electrodes differs across sessions: "154a" and "154b" indicate the sets of electrodes that have been recorded in only a subset of the sessions, while "154" indicates the set of electrodes that has been recorded in every session.

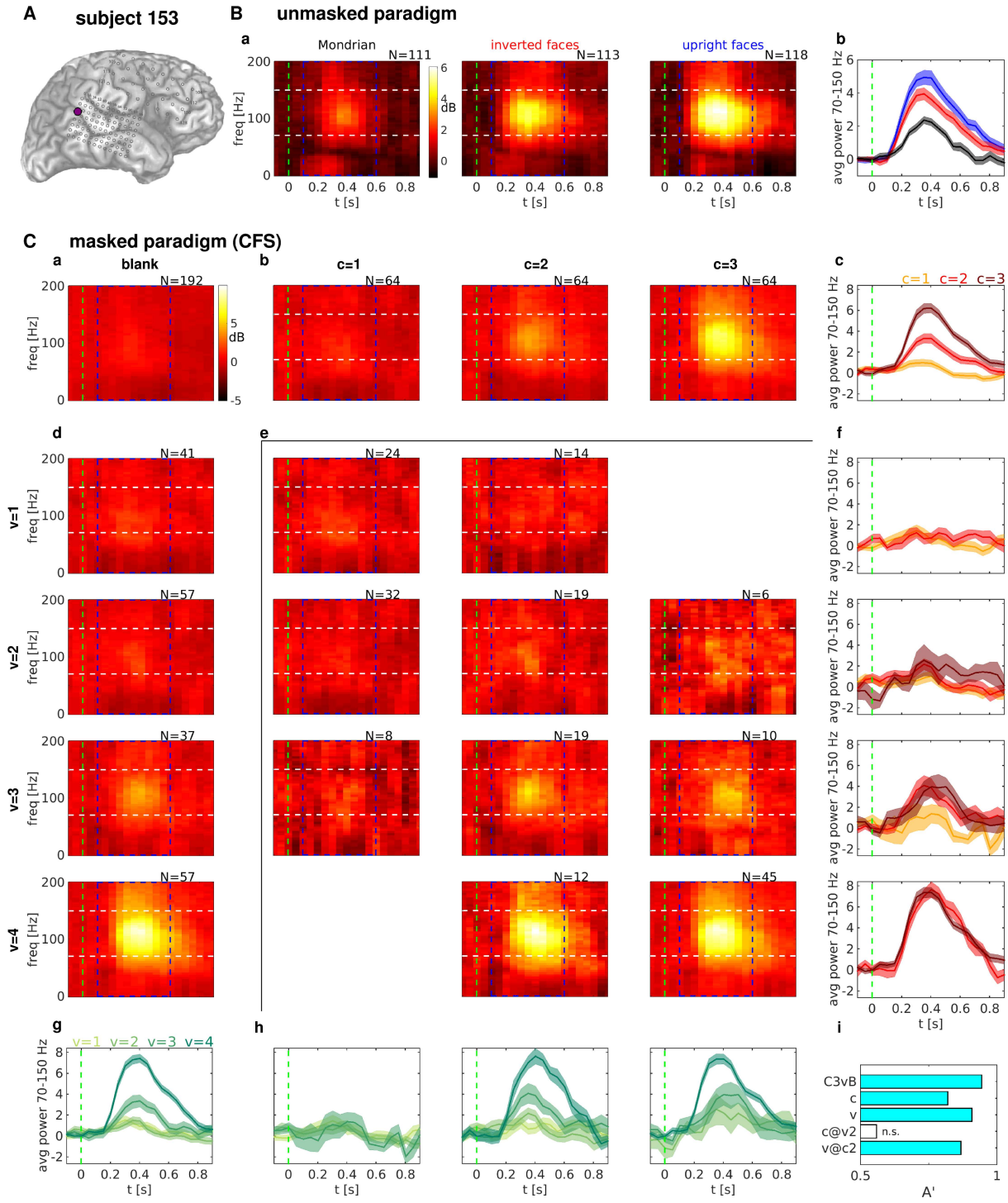

Figure S3. Spectral power responses in the unmasked and CFS experiment for an example electrode in the inferior parietal cortex. Spectral power responses in the unmasked and CFS experiment for an example electrode. Format as in Figure 3.

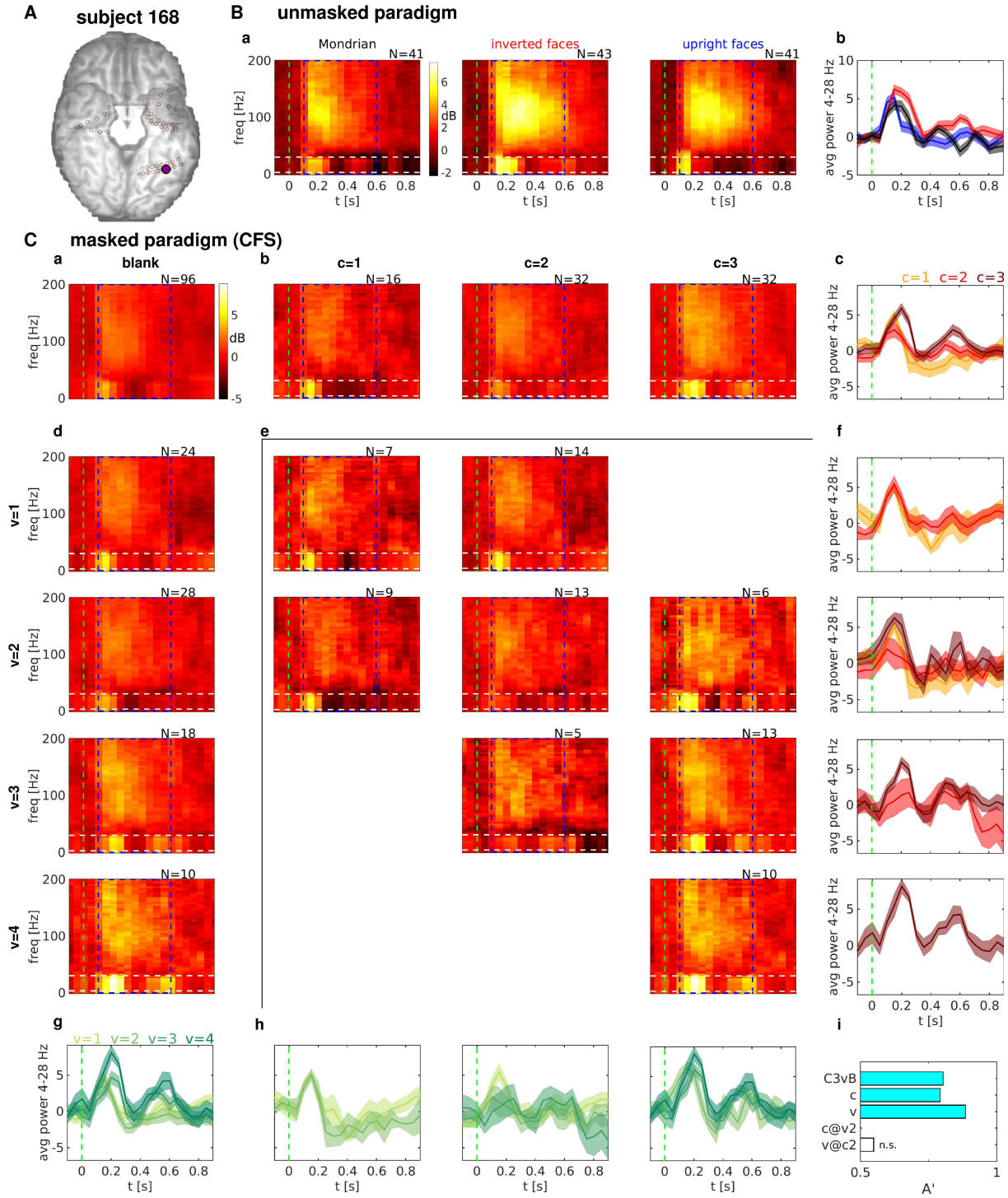

Figure S4. Spectral power responses in the unmasked and CFS experiment for an example electrode in the fusiform gyrus. Spectral power responses in the unmasked and CFS experiment for an example electrode. Format as in Figure 3. The trials with face contrast value c=4 have not been considered for this figure.

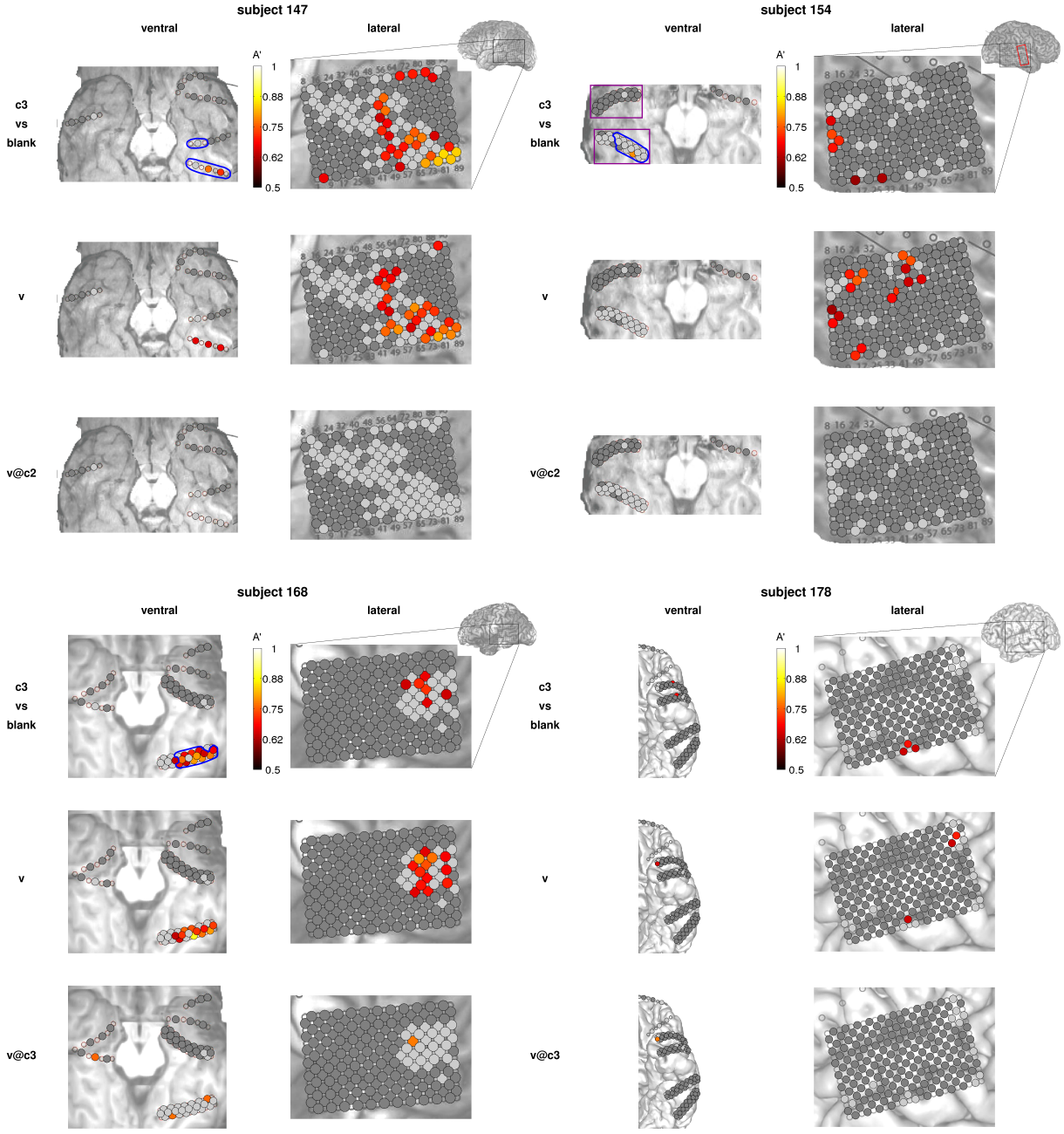

Figure S5. Decoding accuracies in the masked paradigm. Decoding accuracies A' for each electrode are shown color-coded on the ventral and lateral brain images for the remaining four subjects. Same format as in Fig. 4A. For subject 154, different electrodes were recorded on different sessions: the red rectangle in the lateral temporal area indicates the electrodes that have been recorded in the sessions corresponding to "154a" only, and the purple rectangles in the ventral temporal area indicate the electrodes that have been recorded in the sessions corresponding to "154b" only. The other electrodes have been recorded in every session.

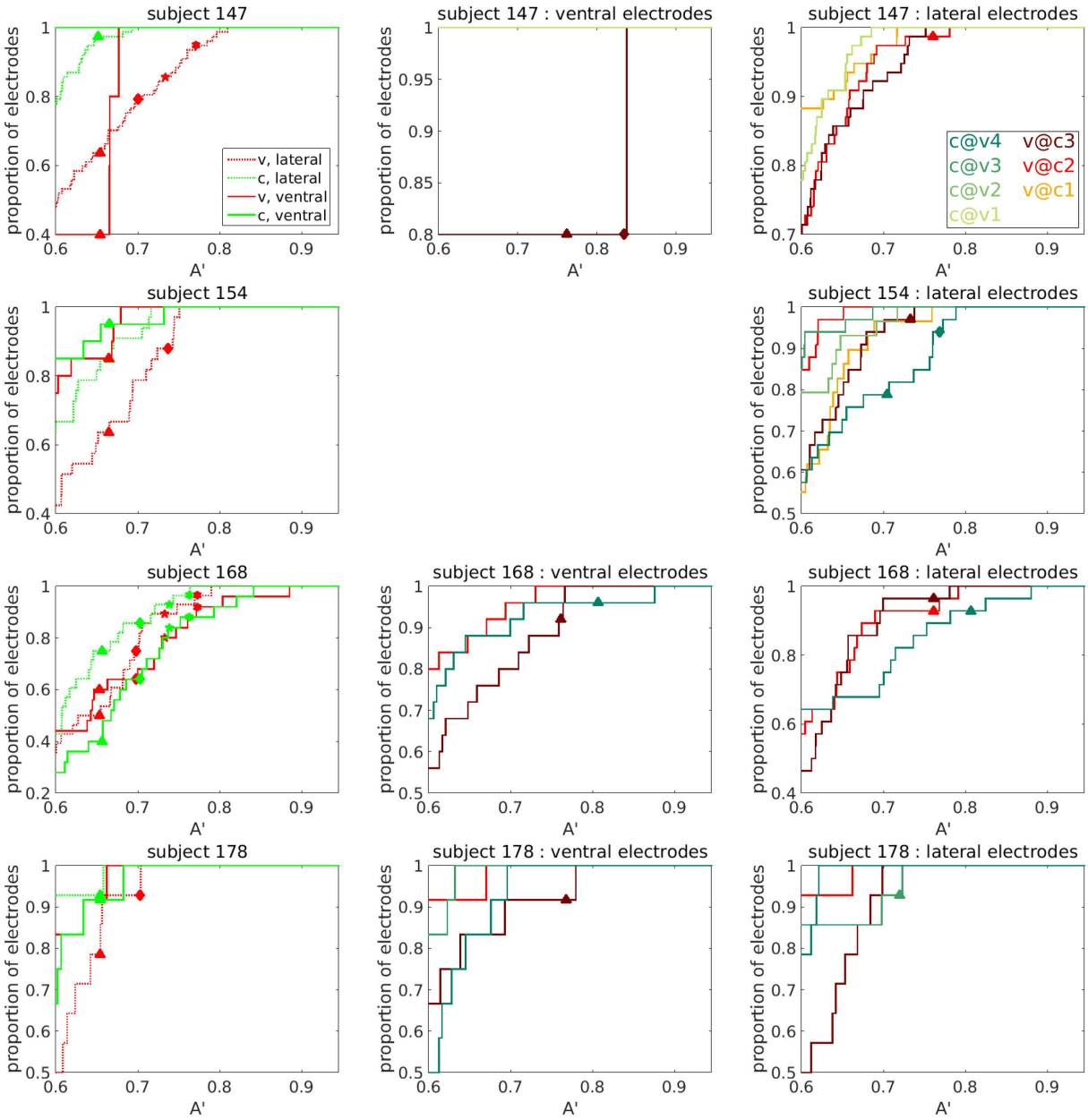

Figure S6. Cumulative probability density functions of decoding accuracy over the populations of ventral and lateral electrodes. Same format as in Fig. 6B, for the remaining subjects. Only results from decoding analyses with at least 10 trials in the least populated class are shown. For subject 154, the numbers of electrodes considered are different for each decoding analysis, as indicated in Fig. S2 and S5. For this subject, none of the face-responsive electrodes located in the ventral cortex have enough trials to compute $v@c$ or $c@v$ decoding, hence the corresponding panel is not shown.

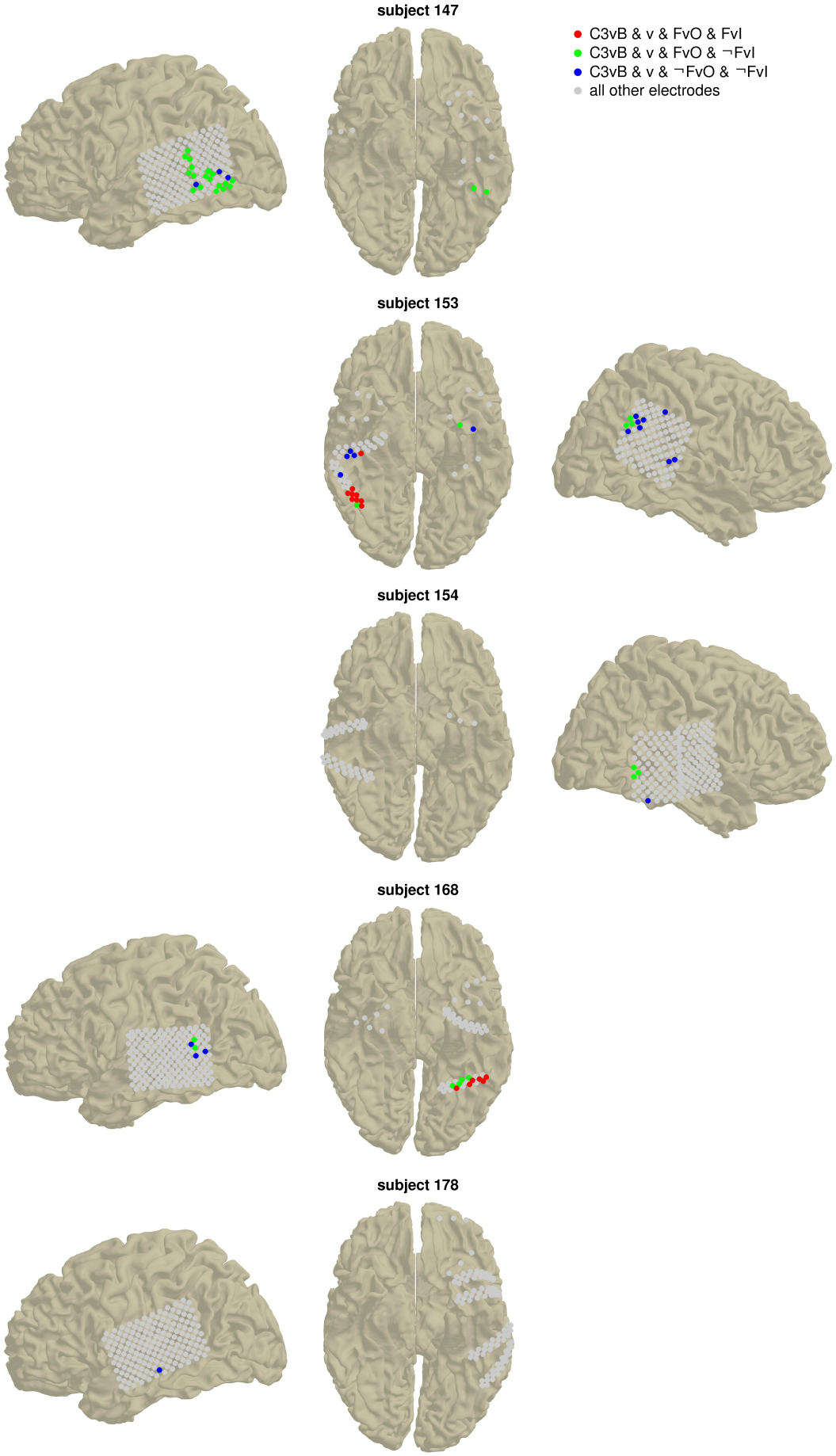

Figure S7. Conjunction of significant decoding results in the masked and unmasked paradigms for each subject. As in Fig. 9, for each individual subject. Note that the FvI (upright vs. inverted face) decoding was not possible for subjects 147 and 178.

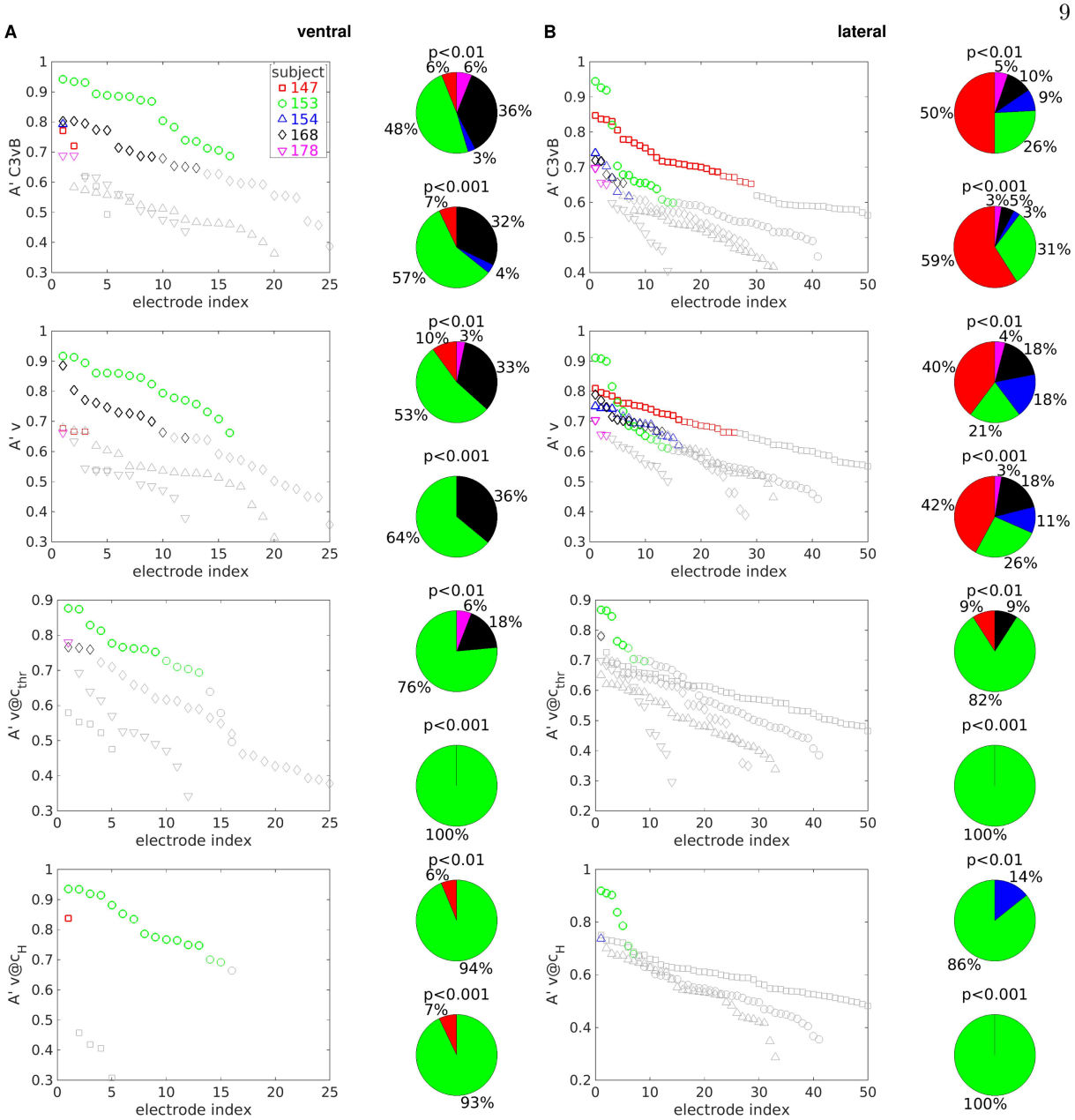

Figure S8. Heterogeneity of decoding results across subjects in the masked paradigm. (A) Decoding accuracies A' for each subject and each face-responsive ventral electrode are shown in descending order. Thick (thin) colored symbols indicate significant decoding accuracy at p<0.001 (p<0.01), gray symbols indicate non-significant decoding accuracy (p>0.01). Colors as in Fig. 2A-D, symbols as in Fig. 5A. Pie charts show the proportion of significant (p<0.01, top; p<0.001, bottom) face-responsive ventral electrodes contributed by each subject for each decoding analyses. From top to bottom: c_3 *vs. blank*, v, $v@c_{\mathrm{thr}}$, $v@c_{\mathrm{H}}$. (B) As in A, for face-responsive lateral electrodes. For subject 147, only the 50 electrodes with the highest A' are shown.

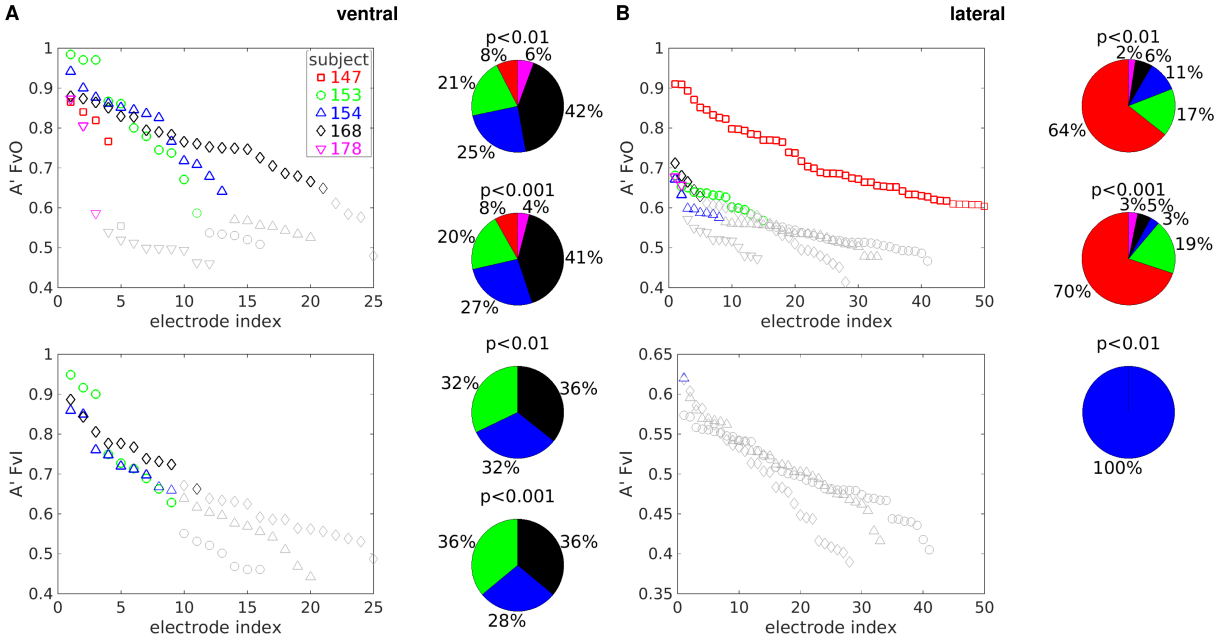

Figure S9. Heterogeneity of decoding results across subjects in the unmasked paradigm. (A) Decoding accuracies A' for each subject and each face-responsive ventral electrode are shown in descending order. Thick (thin) colored symbols indicate significant decoding accuracy at p<0.001 (p<0.01), gray symbols indicate non-significant decoding accuracy (p>0.01). Colors as in Fig. 2A-D, symbols as in Fig. 5A. Pie charts show the proportion of significant (p<0.01, top; p<0.001, bottom) face-responsive ventral electrodes contributed by each subject for each decoding analyses. From top to bottom: upright face vs. other categories, upright vs. inverted face. (B) As in A, for lateral electrodes. For subject 147, only the 50 electrodes with the highest A' are shown.

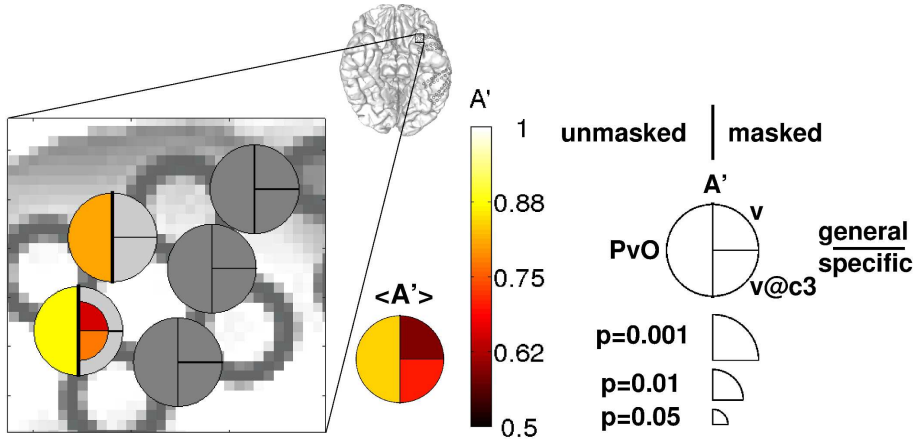

Figure S10. Comparison between masked and unmasked presentations: example of a visibility discriminant and face discriminant electrode located in the temporal pole. Same format as in Fig. 7A, for a set of face discriminant electrodes from the temporal pole of subject 178.